Revisiting neutron studies of reentrant spin glasses: the role of small-angle scattering

Isabelle Mirebeau, Nicolas Martin

JOURNAL OF APPLIED CRYSTALLOGRAPHY

ISSN 1600-5767

Revisiting neutron studies of reentrant spin glasses: the role of small-angle scattering[1]

Isabelle Mirebeau and Nicolas Martin*

Université Paris-Saclay, CNRS, CEA, Laboratoire Léon Brillouin, 91191 Gif-sur-Yvette, France. *Correspondence e-mail: nicolas.martin@cea.fr

Received 28 March 2022
Accepted 6 July 2022

Edited by A. Michels, University of Luxembourg, Luxembourg

[1] This article is part of a virtual special issue on *Magnetic small-angle neutron scattering – from nanoscale magnetism to long-range magnetic structures*.

Keywords: neutron scattering; small-angle neutron scattering; reentrant spin glasses.

The application is discussed of neutron methods to the study of reentrant spin glasses (RSGs), close to the transition towards a 'canonical' spin glass (SG). The focus is on two emblematic systems, namely $Au_{1-x}Fe_x$ and amorphous a-$Fe_{1-x}Mn_x$. A set of experimental results is presented to highlight their peculiar static and dynamic properties. The role of small-angle neutron scattering (SANS) is stressed as an important tool to unravel the structure of these complex systems over mesoscopic length scales. Finally, recent SANS results performed under an applied magnetic field in the region of the RSG → SG transition are presented. They show that vortex-like defects are present in the RSG region up to the critical line and vanish in the SG region. These defects, which develop only in a ferromagnetic medium, could be a key feature to probe the emergence of long-range magnetic order.

1. Introduction

The 2021 Nobel Prize in Physics, co-awarded to G. Parisi 'for the discovery of the interplay of disorder and fluctuations in physical systems from atomic to planetary scales', underscores the importance of a theoretical and experimental study of complex systems. Spin glasses (SGs) are among the best and most studied archetypes of such complexity. The SG state was first discovered in alloys where magnetic impurities are embedded into a non-magnetic metallic matrix. The randomness of their spatial distribution combined with the oscillating nature of the sign of their interaction results in a peculiar kind of magnetic frustration. As a consequence, SGs show a proliferation of energetically equivalent states, each possessing its own dynamics. Their energy landscape is rugged, with multiple minima ('wells') separated by large barriers. This leads to a plethora of interesting experimental phenomena, such as large magnetization irreversibilities, time-dependent susceptibility, ageing, rejuvenation *etc.* (Vincent & Dupuis, 2018). In general, when ferromagnetic (FM) interactions become dominant but compete with antiferromagnetic (AFM) ones, frustrated ferromagnets called reentrant spin glasses (RSGs) show many anomalies akin to 'canonical' SGs.

In this paper, we review some neutron results obtained in metallic systems, where a transition between SG and RSG states can best be studied. Some general aspects of the (R)SGs are first introduced (Section 2). We then describe the search for an order parameter in (R)SGs (Section 3), as well as the dynamic properties of these systems (Section 4). The application of small-angle neutron scattering (SANS) to this kind of problem is discussed in zero and finite applied

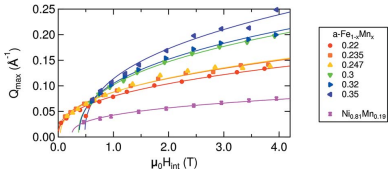

magnetic fields, showing that the method is an excellent tool to investigate the subtle differences between the two ground states (Sections 5 and 6). Finally, we sketch some lines of research which could be pursued thanks to recent developments of SANS-like techniques (Section 7).

2. Physical framework

The main ingredient at the origin of SG behaviour is the combination of randomness and frustrated competing interactions in a magnetic material (Mydosh, 2015). The disorder present in SGs is said to be 'quenched', meaning that the coupling terms J_{ij} between connected spins $\mathbf{S}_{i,j}$ are constant on the time scale over which the $\mathbf{S}_{i,j}$ fluctuate (Castellani & Cavagna, 2005). This is translated in the definition of the Hamiltonians used to describe the main interactions at play in SGs, such as the one used in the Ising mean-field (MF) model of Sherrington and Kirkpatrick (SK) (Sherrington & Kirkpatrick, 1975),

$$\mathcal{H} = -\tfrac{1}{2}\sum_{i\neq j} J_{ij}\,\mathbf{S}_i\cdot\mathbf{S}_j - \mathbf{H}\cdot\sum_i \mathbf{S}_i. \tag{1}$$

Here the first sum runs over all spin pairs in the system (*i.e.* interactions are infinite ranged) and the exchange constants J_{ij} are randomly distributed according to a Gaussian law,

$$p(J_{ij}) = \frac{\exp\left[-(J_{ij}-J_0)^2/2J^2\right]}{J(2\pi)^{1/2}}. \tag{2}$$

The second sum in equation (1) (Zeeman term) runs over each individual spin, subjected to a magnetic field $\mathbf{H}$. The situation where $J_0 \simeq 0$ – or at least is smaller than the variance J^2 of $p(J_{ij})$ – corresponds to the 'canonical' SG ground state. It is realized in alloys obtained by diluting magnetic impurities (Co, Ni, Fe, Mn *etc.*) in a non-magnetic metallic matrix (Ag, Au, Cu *etc.*) at such a low concentration that the impurities are randomly distributed. The impurity spins interact through Ruderman–Kittel–Kasuya–Yosida (RKKY) interactions mediated by conduction electrons, the sign of which oscillates with the distance between them. The presence of quenched disorder, together with the coexistence of FM ($J_{ij} > 0$) and AFM ($J_{ij} < 0$) interactions which nearly compensate on average, yields the SG ground state. Such systems are characterized by the absence of long-range magnetic order (LRMO) even at very low temperature. They also show memory effects and hysteresis, like other vitreous systems. Strikingly, in spite of their metastable character, a transition from the paramagnetic (PM) state (where spins fluctuate randomly in time) to the SG state (with static or 'frozen' disorder) can be shown at a finite temperature T_F.

The first indication of an SG transition was the 'cusp' of the static susceptibility versus temperature observed in dilute Au–Fe alloys (Cannella & Mydosh, 1972). Other clear-cut demonstrations of a genuine – although uncommon – phase transition were found later on. One can quote the frequency-dependent susceptibility (Souletie & Tholence, 1985; Beauvillain *et al.*, 1986) and the divergence of the nonlinear magnetization components (Bouchiat, 1986), among others. The discovery of the SG transition stimulated the introduction of new concepts in condensed matter physics, such as the Edwards–Anderson (EA) parameter q_{EA} which characterizes the SG freezing below T_{SG} in the limit of infinite time t and system size N (Edwards & Anderson, 1975),

$$q_{EA} = \lim_{t\to\infty}\lim_{N\to\infty}\left[\langle \mathbf{S}_i(t_0)\,\mathbf{S}_i(t_0+t)\rangle\right]_{av}, \tag{3}$$

where $[\cdots]_{av}$ and $\langle\cdots\rangle$, respectively, denote the configurational and thermal average, and the concept of magnetic frustration induced by the competition of interactions with opposite signs (Toulouse, 1977).

Historically, the work of EA was almost immediately followed by that of SK mentioned above. The SG problem was not yet solved, however, because the SK solution was shown to yield negative entropies at low temperature by de Almeida and Thouless (AT) (de Almeida & Thouless, 1978). It was only thanks to the work of Parisi (1979), using what is now known as the replica symmetry breaking (RSB) scheme, that a stable solution was found. A full account of these 'heroic' theoretical efforts is beyond the scope of this paper, and we have skipped over other important approaches such as the (short-range) droplet model (Fisher & Huse, 1986) or the chirality scenario (Kawamura, 1992). For pedagogical *entrées* to the SG problem, we refer the reader to the popular series by Anderson – starting with Anderson (1988) – or the recent review paper by Mydosh (2015), which includes theoretical and experimental aspects.

Let us now turn to the following question: What happens when the concentration of magnetic atoms x increases? In the dilute limit (*i.e.* for small x), due to the oscillatory nature of the RKKY interaction occurring in metallic SGs with characteristic periods of a few ångströms, single-atom thermodynamic properties deduced from the partition function $Z = \mathrm{Tr}[\exp(-\mathcal{H}/k_B T)]$ can be expressed as a 'universal' function of the reduced variables T/x and H/x (k_B is the Boltzmann constant). Therefore, the knowledge of the system for a given x is sufficient to deduce its behaviour for other concentrations through this simple scaling (Souletie & Tournier, 1969; Souletie, 1978).

In real concentrated systems, however, two main phenomena occur for the magnetic atoms: (i) they interact via short range interactions, such as direct exchange for instance, and (ii) they are not distributed fully randomly such that some local configurations can be favoured. The features are usually precursors of another ground state, called reentrant spin glass (RSG), which can at first sight be described as a frustrated disordered ferro- or antiferromagnet, depending on the sign of the dominant interaction. From now on, we shall focus on the FM case.

The transition from SG to RSG was studied theoretically by Gabay and Toulouse (GT) (Gabay & Toulouse, 1981) through an MF approach using the EA order parameter and the replica method already used by SK. Their picture yields a phase diagram (J_0, T), shown in Fig. 1 for the case $m = 3$ (Heisenberg

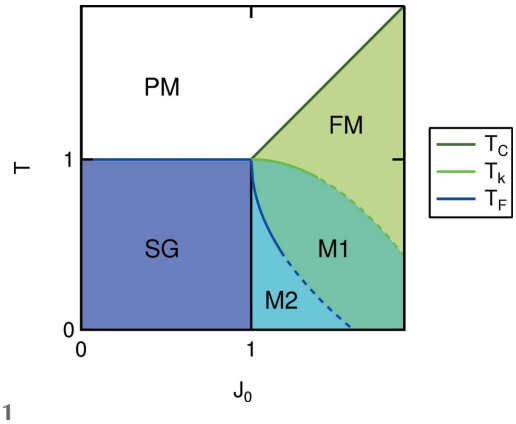

Figure 1
Mean-field phase diagram for a bond-disordered ferromagnet calculated using the model of Gabay & Toulouse (1981) for Heisenberg spins. The various transition temperatures are indicated for further reference. Dashed lines illustrate the fact that the obtained M2 ↔ M1 and M1 ↔ FM transition lines are only exact close to the multicritical point (*i.e.* for $J_0 \gtrsim 1$).

spins). It is marked by a multicritical point located at $T = J_0 = 1$ and a vertical line between RSG and SG phases. For $J_0 > 1$ (*i.e.* in the RSG region), lowering the temperature leads to the occurrence of two mixed phases M1 and M2, where SG and FM order parameters coexist microscopically. At each magnetic site, a longitudinal spin component forming LRMO coexists with a transverse one, randomly oriented in the perpendicular plane. Upon cooling, the transitions from FM to M1 and M2 phases are characterized by the occurrence of a static transverse spin component associated with weak irreversibilities (for M1) and strong irreversibilities involving the 'replica symmetry breaking' scheme of Parisi (for M2). The transition temperature from FM to the M1 phase occurs at the canting temperature T_k,[2] whereas that from M1 to M2 occurs at the freezing temperature T_F. This latter transition line is formally analogous to the AT transition predicted for spin glasses in a magnetic field (de Almeida & Thouless, 1978; Toninelli, 2002). However, we note that, in the GT model, LRMO is preserved down to the lowest temperatures, so that the $T = 0$ transition from RSG to SG ground state at $J_0 = 1$ corresponds to the breakdown of the LRMO.

The huge success of the GT model is explained by the fact that this theoretical phase diagram seems to map quite well to the experimental ones obtained in a great variety of systems, whatever the nature of their chemical disorder or crystal structure, or the range of the competing magnetic interactions. An example is given in Fig. 2 for the amorphous $(Fe_{1-x}Mn_x)_{75}P_{16}B_6Al_3$ system (hereafter named a-$Fe_{1-x}Mn_x$ for the sake of brevity), where the phase diagram is inferred from a.c.-susceptibility measurements.

In practice, the parameter which monitors the distribution of interactions is usually the concentration of a magnetic atom x (with a critical value x_C corresponding to $J_0 = 1$), but it could also be a thermodynamic parameter, such as pressure in systems prone to an instability of the band structure. However,

[2] T_k should not be confused with the Kondo temperature T_K.

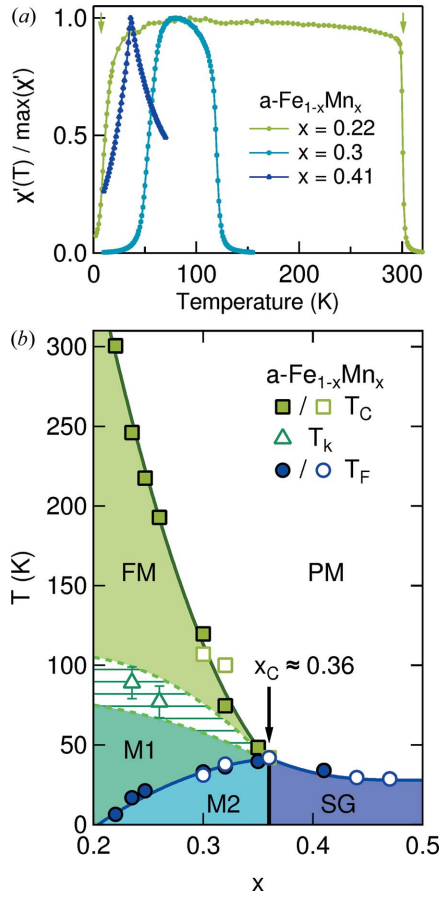

Figure 2
(*a*) The zero-field a.c. susceptibility of a-$Fe_{1-x}Mn_x$ for x = 0.22, 0.3 and 0.41, recorded under an a.c. field of 10 Oe amplitude and 1 kHz frequency [data taken from Martin *et al.* (2021)]. The Curie (T_C) and freezing (T_F) temperatures are defined as the high- and low-temperature inflection points, respectively (as shown by the arrows for x = 0.22). (*b*) A phase diagram reconstructed from such data. T_C and T_F values are from Martin *et al.* (2021) (solid symbols) and Yeshurun *et al.* (1980) (empty symbols). T_k is determined from Mössbauer spectroscopy and muon spin relaxation (μSR) (Mirebeau *et al.*, 1986, 1997).

since the experimental phase diagrams are usually deduced from macroscopic measurements, such as low-field magnetization, they do not provide a direct insight into the spin correlations.

Therefore, when comparing experimental and theoretical phase diagrams, some questions still arise, which have been strongly debated in the past: Is LRMO really preserved in the whole RSG ground state up to x_C, as predicted? What is occurring when approaching x_C? Is there a vertical transition line from RSG to SG states or only a gradual change of the microscopic magnetic state? Neutron scattering, and especially SANS, provides crucial answers to these questions by investigating the (R)SG state at a microscopic level, both in zero and in an applied magnetic field. In the following, we review some of these results, focusing on two emblematic metallic systems, namely $Au_{1-x}Fe_x$ and a-$Fe_{1-x}Mn_x$, with dominant FM interactions in the RSG region. We will also briefly touch upon canonical SGs, taking the archetypal $Cu_{1-x}Mn_x$ system as an example, to describe the main

experimental findings made in this context and highlight the differences with respect to RSGs.

3. Order parameter in (R)SGs: the neutron viewpoint

3.1. Reentrant spin glasses

LRMO is usually detected by conventional (wide-angle) neutron diffraction which is sensitive to the magnetic Bragg contribution to the scattering pattern. However, in the RSGs considered here, such measurements are quite complex and their interpretation non-trivial, as discussed later. On the other hand, investigating the presence of magnetic domains is a good alternative way to check for the presence of LRMO.

In a non-frustrated ferromagnet, FM exchange and anisotropy terms compete with dipolar interactions on the microscopic scale. In zero magnetic field, this competition results in the onset of large magnetic domains (typically micrometre sized) over which the internal magnetization is preserved, whereas the domain configuration minimizes magnetostatic and anisotropy energies. To handle the question of LRMO in RSGs, one could therefore explore whether such large domains can be observed or if LRMO is actually broken on a much shorter scale.

Polarized neutrons can probe FM domains by studying the depolarization of the transmitted beam. A small guide field (a few oersted, or even less for long-wavelength neutrons) is necessary to keep the initial neutron polarization. Along the sample path, neutron spins precess in the magnetic field induced by a domain, then are subjected to a non-adiabatic process when crossing a Bloch wall, and so on. The succession of such events induces a loss of polarization, providing information about domain sizes (Halpern & Holstein, 1941; Mitsuda & Endoh, 1985). This technique, initially used in standard ferromagnets, was successfully applied to FM RSGs (Mirebeau *et al.*, 1990; Sato *et al.*, 1993). Fig. 3 displays the result of such a measurement performed on a-$Fe_{1-x}Mn_x$ foils,

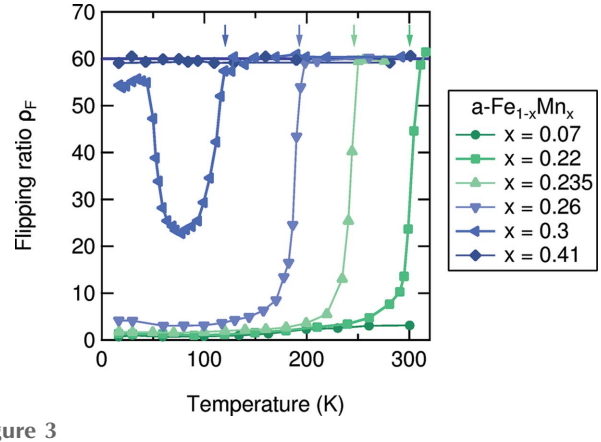

Figure 3
Spin depolarization measurements performed on a-$Fe_{1-x}Mn_x$ ribbons with varying concentrations $0.07 \leq x \leq 0.41$, using neutrons of wavelength $\lambda = 5$ Å and under an applied field $H = 5$ Oe [data taken from Mirebeau *et al.* (1990)]. The thickness d of the samples is situated in the range 25–70 µm.

i.e. the beam 'flipping ratio' ρ_F which is related to the beam polarization P by $\rho_F = (1 + P)/(1 - P)$. In the weakly frustrated limit (RSG samples with $x \ll x_C \simeq 0.36$), micrometre-sized domains can be evidenced by a strong depolarization of the transmitted neutron beam below T_C, as for conventional ferromagnets. On the other hand, in the SG sample ($x = 0.41 > x_C$, no depolarization occurs even below T_{SG}, due to the non-adiabatic transitions undergone by the neutron spin in the varying magnetic field created by the locally ordered frozen moments (*i.e.* as would be the case in the PM state).

The behaviour for samples with $x \simeq x_C$ deserves detailed study. ρ_F (or P) either shows a plateau [$Ni_{1-x}Mn_x$ (Sato *et al.*, 1993), a-$Fe_{1-x}Zr_x$ (Hadjoudj *et al.*, 1991)] or a minimum [a-$Fe_{1-x}Mn_x$ (Mirebeau *et al.*, 1990), $Au_{1-x}Fe_x$ (Mitsuda *et al.*, 1991)] at low temperatures. These observations indicate two types of FM RSG, namely 'rigid ones' (where LRMO, and thus ρ_F, are not affected by temperatures below T_C) and 'non rigid' ones (where a partial breakdown of the LRMO occurs in the mixed phases, yielding an increase in ρ_F below T_F). These two behaviours are connected with the strength of the Dzyaloshinskii–Moryia (DM) anisotropy field (Mirebeau *et al.*, 1992). Note that the domains have also been observed by electron microscopy (Senoussi *et al.*, 1988) and, more recently, acoustic damping measurements (Kustov *et al.*, 2017), confirming the global validity of the MF model, at least in FM RSGs far from the critical region.

In addition to the effects discussed above, the onset of LRMO below T_C yields a magnetic Bragg contribution superimposed on the 'nuclear' contribution coming from the crystallographic order. Following this contribution as a function of T and x should, in principle, yield unambiguous answers about the order parameter in the RSG ground state, the mixed phases and across the $T = 0$ transition at x_C. The situation is actually not so simple in 3*d* metals, where magnetic moments are partly delocalized and much smaller than *e.g.* in rare earths, so that the FM contribution to the Bragg peaks can be very weak, even in a non-frustrated ferromagnet or in the weakly frustrated regime. As a prominent example, a careful investigation of the magnetic Bragg intensity was performed by Murani (1980) in two $Au_{1-x}Fe_x$ RSG samples in zero magnetic field. The phase diagram of $Au_{1-x}Fe_x$ [Fig. 4(*a*)] is reminiscent of that of a-$Fe_{1-x}Mn_x$ [Fig. 2(*b*)], with a critical concentration $x_C \simeq 0.16$ depending on the heat treatment of the samples, and separating the SG ($x < x_C$) and RSG ($x > x_C$) regimes. In the RSG sample with $x = 0.19$, the magnetic Bragg intensity *increases* below T_C down to the lowest measured temperature, with two anomalies at $T_1 \simeq 45$ K and $T_2 \simeq 125$ K [Fig. 4(*b*)]. Notably, no breakdown of the LRMO is observed, in agreement with MF predictions. Unfortunately, such measurements have not been performed in $Au_{1-x}Fe_x$ closer to x_C or in most metallic systems. This is mostly due to the very small FM signal, even in single-crystalline samples. For instance, the magnetic contribution is of the order of 10^{-2} of the nuclear contribution in $Au_{1-x}Fe_x$ [see Fig. 4(*b*)] and goes down to $\sim 10^{-4}$ in another emblematic system, $Ni_{1-x}Mn_x$, with much smaller magnetic moments (Cable & Child, 1974). In amorphous samples such as a-$Fe_{1-x}Mn_x$, the lack of structural

periodicity leads to broad nuclear 'peaks', rendering the analysis complex and hardly meaningful.

On the other hand, the use of polarized neutrons can drastically enhance the magnetic contribution at the Bragg peak position, but requires the application of a magnetic field, leading to the saturation of the sample. Such data are plotted in Fig. 4(*b*) for the same $Au_{1-x}Fe_x$ (x = 0.19). One can see that an applied field of 2 T is sufficient to erase the low-temperature features on the T dependence of the Bragg peak intensity reported by Murani (1980). In particular, this tends to contradict the scenario stating that the anomaly at T_2 is due to the onset of next-nearest-neighbour (NNN) couplings J_2 (Brout, 1959). The latter can be estimated as $J_2 \simeq k_B T_2/z_2 \simeq$ 1.8 meV atom^{-1}, where $z_2 = 6$ is the NNN lattice connectivity in face-centred cubic $Au_{0.81}Fe_{0.19}$. This value is therefore much larger than the Zeeman energy calculated for an Fe moment $\mu_{Fe} \simeq 3.2\ \mu_B$ atom^{-1} (Wilhelm *et al.*, 2008) in a 2 T field (∼0.4 meV atom^{-1}), suggesting other origins for the observed anomalies. In order to gain a deeper insight into this interesting puzzle, one could perform a systematic study of the temperature and field dependence of the magnetic Bragg scattering or try to evaluate the exchange constants $J_{1,2}$ using inelastic neutron scattering.

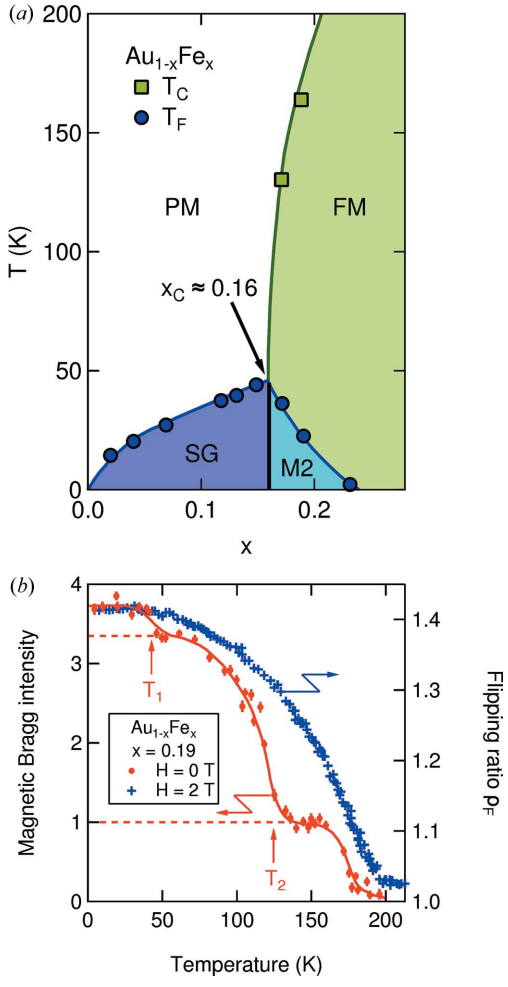

Figure 4
(*a*) An (x, T) phase diagram of $Au_{1-x}Fe_x$ deduced from magnetic susceptibility measurements. Data points are taken from Belokon' *et al.* (2006). (*b*) The temperature dependence of the zero-field magnetic (111) Bragg intensity for the $Au_{1-x}Fe_x$ (x = 0.19) RSG alloy, given as a percentage of the underlying nuclear intensity [red circles, data taken from Murani (1980)]. Blue crosses show the temperature dependence of the magnetic flipping ratio ρ_F obtained under an applied field of 2 T with neutrons of wavelength λ = 0.865 Å (5C1 diffractometer at Laboratoire Léon Brillouin), recalling that $\rho_F \simeq 1 + 4\alpha$, where α is the magnetic to nuclear structure factor ratio, in the limit $\alpha \ll 1$.

3.2. Spin glasses

In SGs, LRMO is by definition destroyed. Situations where spins are in a fully random state are, however, very seldom found in nature. Moreover, most solid solutions of binary alloys tend to display atomic short-range order, as shown by diffuse scattering studies using unpolarized and polarized neutrons (Cable *et al.*, 1982; Harders *et al.*, 1983; Mirebeau *et al.*, 2019). This point must be considered when analysing the magnetic properties of 'real life' SGs.

As a consequence, spin correlations usually persist at length scales which vary with sample and temperature, typically from the scale of interatomic distances up to dozens of nanometres. These short-range correlations can be of FM or AFM type, inducing weak modulations of the neutron cross section. An increase in the forward scattering is observed in the SANS region in the FM case, or a broad feature at the positions expected for the AFM Bragg peaks in the AFM case.

Neutron diffraction measurements show the progressive development of these correlations as the temperature decreases from the paramagnetic state ($T \gg T_F$). Their freezing is shown by a blocking of the correlation length at temperatures slightly above T_F. A good example is the model $Cu_{1-x}Mn_x$ SG where short-range helical correlations were studied in detail by Cable *et al.* (1982) and Tsunoda & Cable (1992).

The measurement of the EA parameter [q_{EA} defined by equation (3)] which develops below T_F is not directly accessible to neutron diffraction, namely without energy analysis of the diffracted neutron beam (Hicks, 1983). On the other hand, the evolution of the spin dynamics can be followed above and below T_F using neutron spin echo (NSE) or quasi-elastic neutron scattering (QENS). Both techniques show the onset of a static order parameter at the relatively short neutron time scale (10^{-12} to 10^{-8} s) and for the nanometric length scale probed in the investigated Q range [$Q = (4\pi/\lambda)\sin(\theta/2)$, where θ is the scattering angle and λ is the wavelength of the incident radiation]. In $Cu_{1-x}Mn_x$ (x = 0.05, T_F = 27.4 K), the time correlation of an Mn moment, related to q_{EA}, was followed over a huge time window (12 orders of magnitude) by combining NSE, muon spin relaxation (μSR) and a.c. susceptibility (Mezei & Murani, 1979; Uemura *et al.*, 1984). Similar determinations of the EA order parameter were performed in $Au_{1-x}Fe_x$ (x = 0.01) by comparing Mössbauer and μSR data, with typical time scales of 10^{-9} and 10^{-6} s, respectively (Uemura *et al.*, 1980; Hartmann-Boutron, 1982). In the concentrated SG a-$Fe_{1-x}Mn_x$ (x = 0.41), the onset of the EA parameter and the freezing dynamics of the fluctuating

spins were studied by combining QENS and three-axis (TAS) spectrometry (see Section 4).

4. Spin dynamics

4.1. Spin wave spectrum in RSGs

In FM RSGs, spin waves (SWs) are observed below T_C, similar to non-frustrated ferromagnets. They can clearly be detected by inelastic neutron scattering (INS) through an energy analysis of the magnetic cross section in the momentum transfer range $10^{-2} < Q < 10^{-1}$ Å^{-1}. INS patterns show two SW peaks at finite energy transfers $\pm\hbar\omega_0$ on each side of the elastic peak ($\hbar\omega = 0$), which correspond to the creation and annihilation of an SW. Assuming a given form of the spectral function, a measurement of the dispersion law ($DQ^2 + \Delta$) provides the values of the stiffness constant D and anisotropy gap Δ, whereas the intrinsic broadening of the SW peaks gives access to the damping constant Γ (half-width at half-maximum of a Lorentzian spectral function). SWs are strongly damped by frustration and magnetic disorder, and both D and Γ show temperature anomalies in the region of T_k and T_F (B. Hennion *et al.*, 1986). Namely, D shows a minimum when entering the M1 phase at T_k, further increasing or saturating in the M2 phase, whereas Γ shows the reverse behaviour. Such anomalies have been observed in several systems, including a-$Fe_{1-x}Mn_x$ (Aeppli *et al.*, 1984; B. Hennion *et al.*, 1986), $Ni_{1-x}Mn_x$ (Hennion *et al.*, 1984) and $Fe_{1-x}Cr_x$ (Lequien *et al.*, 1988). They are clearly visible in weakly frustrated samples and persist under an applied magnetic field of a few kilooersted (Hennion *et al.*, 1988). In the strongly frustrated RSGs, when approaching the critical concentration $x \simeq x_C$, Γ becomes comparable to D and the SW peaks tend to merge, yielding a diffusive mode similar to the QENS observed in spin glasses.

4.2. Diffusive mode in SGs

In the 'concentrated' SG a-$Fe_{1-x}Mn_x$ ($x = 0.41 \geq x_C$), where FM correlations develop over finite length scales as the temperature decreases, the neutron intensity is high in the SANS region. The freezing dynamics can thus be studied in detail using QENS and TAS spectrometry. Energy cuts extracted at a given Q value can be modelled using the following expression (Bellouard *et al.*, 1992):

$$S(Q,\omega) = C_1(Q)\,\delta(\omega) + C_2(Q)\,\frac{k_f\,\hbar\omega/k_BT}{k_i\left[\exp(\hbar\omega/k_BT) - 1\right]} \times \frac{\Gamma(Q)/\pi}{\Gamma(Q)^2 + (\hbar\omega)^2}, \quad (4)$$

which allows separation of the elastic intensity (C_1) from the quasi-elastic intensity (C_2), taking into account the transfer function of the spectrometer (through the incident k_i and final k_f neutron wavevectors) and the thermal population factor. In the limit $\hbar\omega \ll k_BT$, C_2 varies as $k_BT\chi(Q)$, where $\chi(Q)$ is the generalized spin susceptibility assuming a Lorentzian line shape. At high temperatures ($T \gg T_F$), *i.e.* in the paramagnetic regime, C_1 varies like a Debye–Waller factor (reflecting atomic vibrations) while C_2 is expected to be roughly T independent [because of the Curie dependence of the high-T spin susceptibility $\chi(Q) \simeq 1/T$ yielding $C_2 \simeq$ constant]. At low temperatures, however, the SG freezing yields anomalies in the T dependence of these parameters [Fig. 5(*a*)] (Bellouard *et al.*, 1992):

(i) An extra contribution of magnetic origin appears on C_1 due to the onset of a non-zero EA parameter.

(ii) Concomitantly, C_2 decreases by the same quantity. The T_F detected here is ∼50 K, *i.e.* above the documented value of ∼34 K inferred from a.c. susceptibility (Martin *et al.*, 2021). This is not surprising, since the length and time scales of the neutron probe are both quite short with respect to macroscopic techniques. For instance, there is a difference of nine orders of magnitude between the two methods (10^{-12} to 10^{-9} s versus 10^{-3} to 10^{-1} s), recalling that T_F typically *increases* with the characteristic measurement frequency.

(iii) More surprisingly, the quasi-elastic width Γ shows a minimum in the region of T_F [Fig. 5(*b*)]. This marked upturn calls for a change in the nature of the spin diffuse excitations above and below T_F.

In order to understand this last result, one can propose a 'handwaving' picture. Above T_F, the spin dynamics are dominated by relaxation modes involving thermally activated

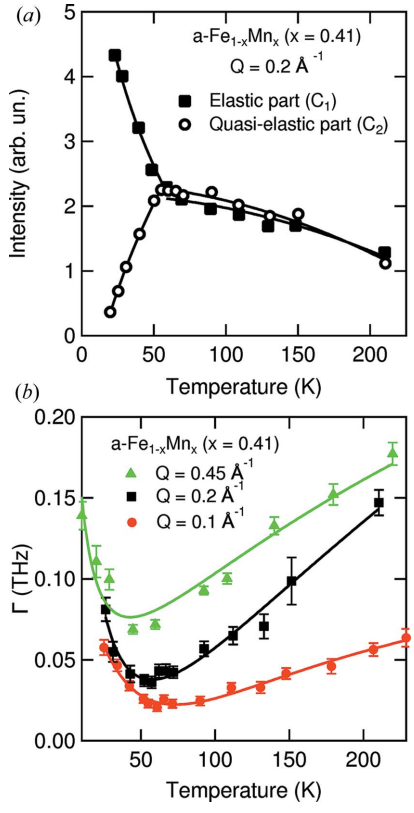

Figure 5
(*a*) The temperature dependence of the elastic (C_1) and quasi-elastic (C_2) parts of the scattered intensity measured using TAS in a-$Fe_{1-x}Mn_x$ (x = 0.41) at Q = 0.2 Å^{-1} (see text). A (constant) negative offset has been applied to C_1 to display both quantities on the same plot. (*b*) The temperature dependence of the quasi-elastic linewidth Γ determined using TAS (Q = 0.1 and 0.2 Å^{-1}) and time-of-flight spectroscopy (Q = 0.45 Å^{-1}). In both panels, data are taken from Bellouard *et al.* (1992).

jumps *between* potential wells, which become more and more rare as T decreases. A decrease in Γ is then related to the inverse relaxation time of these jumps. Below T_F, the excitations take place *within* individual wells, and Γ rather reflects the stiffness of this diffuse excitation, which increases as T further decreases. Such a picture is supported by the study of memory effects and the hierarchical picture of energy wells in SGs (Lefloch *et al.*, 1992). It is also reminiscent of the minimum of the stiffness constant D when entering the M2 phase of the RSG phase diagram described above [Figs. 1 and 2(*b*)].

5. SANS studies in zero magnetic field: on the verge of the Q = 0 Bragg peak

SANS is a popular method for studying objects with characteristic sizes in the 1–1000 nm range within bulk samples. Being ubiquitous in soft matter and biophysics, it can efficiently be applied to magnetic systems showing either long-period structures or magnetic inhomogeneities on the mesoscale (Mühlbauer *et al.*, 2019; Michels, 2021; Honecker *et al.*, 2022). As a consequence, SANS has been extensively used to study SGs and RSGs in the search for magnetic correlations and/or textures. We give here a brief overview of the main results obtained.

5.1. The medium Q range: critical fluctuations and transverse spin freezing

In any ferromagnet, the onset of FM correlations as the temperature decreases and approaches T_C can be observed by SANS, in the range $10^{-2} < Q < 10^{-1}$ Å^{-1}. A standard analysis of the magnetic cross section (including a deconvolution of the experimental resolution function from the data) can be performed using the Ornstein–Zernicke formalism. It yields the FM correlation length which tends to diverge at T_C, thereby leading to the well known peak of critical scattering. The susceptibility deduced from the same fits can be compared with the volumic susceptibility.

In a weakly frustrated FM RSG such as a-$Fe_{1-x}Mn_x$ (x = 0.247), the critical regime appears to be similar to that of a standard ferromagnet (Hennion & Mirebeau, 1995). This is the case for weakly frustrated $Au_{1-x}Fe_x$ (x = 0.18, 0.2) as well, although the critical exponents may be affected (Pappas *et al.*, 1996). The latter is also found to be true for similar systems. This led Haetinger *et al.* (2009) to propose a 'weak' universality class, in which static critical exponents display values lying between those found for classical FM and SG transitions.

On the other hand, in the RSG samples, the behaviour of the SANS cross section below T_C reveals an original feature. An extra SANS intensity starts growing at T_k, *i.e.* well below T_C [Fig. 6(*a*)] (Aeppli *et al.*, 1982). Such an observation was initially interpreted as a sign of the breakdown of the (longitudinal) LRMO, yielding a broadening of the Q = 0 Bragg peak. However, the presence of micrometre-sized domains refutes this interpretation. An alternative explanation can be given in the framework of the GT model.

In this framework, the extra SANS intensity marks the freezing of spin components in the plane transverse to the direction of the longitudinal domain magnetization. Below T_k, transverse spin components become static on the time scale of the neutron probe and correlate ferromagnetically on the scale of a nanometre, so that they can be observed in the same Q range as the critical scattering and the SW contribution. The temperature T_k is then identified with the canting temperature of the GT model, which marks the transition from the FM regime to the mixed M1 phase. When SANS measurements are performed with energy analysis, the contribution of this transverse intensity (which *increases* as temperature decreases) is superimposed on the contribution of thermally activated SWs (which *decreases* as temperature decreases). The coexistence of these two signals partly hampers the determination of T_k. Performing an energy analysis of the diffracted neutron beam suppresses the SW contribution and confirms the static character of the transverse spin correlations, yielding a clear observation of the canted state in zero magnetic field (Mirebeau, 1987). Note that in iron-based systems T_k can also be determined at a local scale thanks to ^{57}Fe Mössbauer spectroscopy (Lauer & Keune, 1982; Mirebeau *et al.*, 1986)

In strongly frustrated RSGs ($x \simeq x_C$), T_C and T_k become very close, and the FM and mixed M1 phases are more difficult to separate. In other words, there is no minimum of the SANS intensity between these two temperatures. Due to this

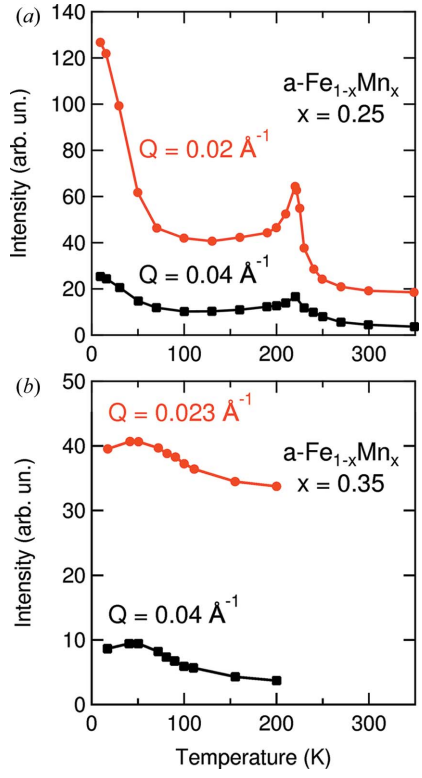

Figure 6
The temperature dependence of the SANS intensity in a-$Fe_{1-x}Mn_x$ for different Q values, (*a*) deep inside the RSG region (x = 0.25) and (*b*) close to the SG regime (x = 0.35). In both panels, data are taken from Aeppli *et al.* (1982).

smearing, SANS in zero magnetic field cannot be used to investigate the existence of a critical point at $T = 0$ or the vertical M2 $\rightarrow$ SG line predicted by MF theories (Fig. 1). Applying a magnetic field partly helps in resolving this difficulty, as discussed in Section 6.

5.2. The very low Q range: Bloch walls and static long-range defects

In the range $10^{-3} < Q < 10^{-2}$ Å^{-1}, the critical scattering peak is no longer observed. SANS in zero magnetic field rather probes very long range static textures, such as magnetic dislocations or Bloch walls. In a non-frustrated ferromagnet, their temperature dependence roughly reflects that of the squared magnetization in a high field, although it may show some thermal irreversibilities. In a-$Fe_{1-x}Mn_x$ and $Au_{1-x}Fe_x$, however, the strong decrease in the intensity observed at low temperature reflects a change in Q dependence of the scattering law associated with these large-scale defects (Mirebeau *et al.*, 1989; Murani, 1980). Theses features are illustrated in Fig. 7 over a Q range spanning one decade.

In order to rationalize the zero-field SANS results, it is interesting to observe the major trends in the T dependences of the scattered intensities for various Q and x values. From small x (*i.e.* weak frustration) and large Q, one observes the peak of critical scattering at T_C and a marked low-temperature increase in intensity below T_k, clearly distinct from the T_C peak [see Figs. 6(*a*) and 7(*b*)]. For samples with $x < x_C$, decreasing Q washes the critical peak away. This is very similar to the effect produced by increasing x towards the SG regime, naturally leading to the disappearance of the features attributable to an ordered structure [compare data obtained at the same Q values in Figs. 6(*a*) and 6(*b*)]. These characteristics give credit to the idea that SANS is mostly sensitive either to dynamic anomalies within ordered domains or to the domain walls themselves, but not directly to the SG order parameter.

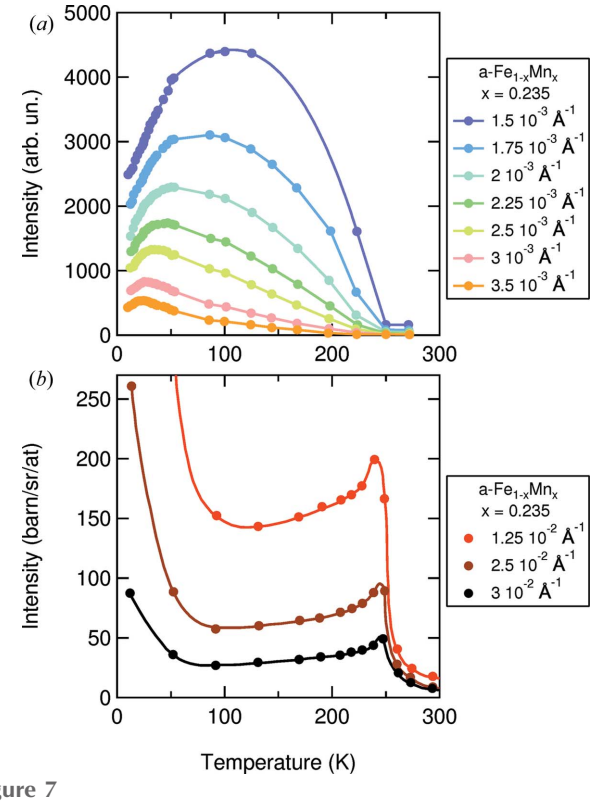

Figure 7
The temperature dependence of the SANS intensity in a-$Fe_{1-x}Mn_x$ (x = 0.235) for (*a*) small and (*b*) medium Q values. In both panels, data are taken from Mirebeau *et al.* (1989) and lines are guides to the eye.

6. SANS under a magnetic field: probing vortex-like defects

To understand the role of an applied magnetic field, one can first compare magnetization curves (Fig. 8) and SANS data (Fig. 9) in a single system where magnetic frustration can be finely tuned. The a-$Fe_{1-x}Mn_x$ series is especially suitable for this study. In these amorphous samples, magnetic disorder is quenched in a reproducible way (*i.e.* it does not require careful thermal treatment, in contrast to single-crystalline materials), so that a fine tuning of the magnetic frustration can be realized by varying the Mn concentration x. We focus here on the low-temperature properties to follow the evolution of the magnetic ground state from RSG to SG.

Let us start with the weakly frustrated x = 0.22 sample in which a transition from an FM state to the low-temperature mixed phase occurs upon cooling [Fig. 2(*b*)]. The magnetization steadily increases when applying small fields (typically up to 0.1–1 kOe) and then reaches a quasi-saturation plateau (Fig. 8). The initial step increase in the magnetization is due to the suppression of large-scale entities – Bloch walls and magnetic dislocations – which disappear as the magnetic domains align along the field direction. This is confirmed by the fact that SANS in the low-Q range is suppressed in the same field range. Such behaviour is similar to that observed in non-frustrated ferromagnets.

When the field increases further, a residual slope of the magnetization persists up to the maximum applied field, even at the lowest temperatures where SW contributions are negligible. This peculiar slope is a macroscopic sign of the progressive field alignment of the transverse spin components

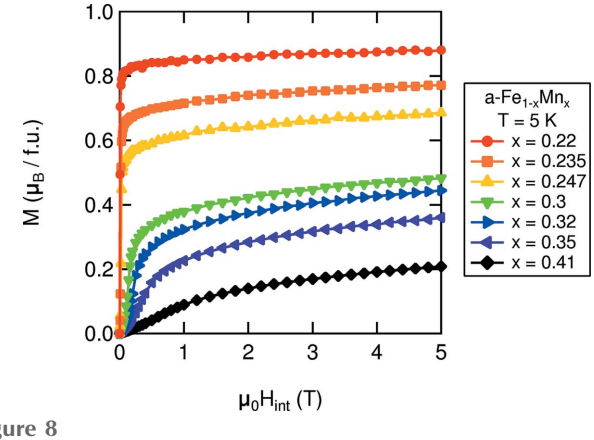

Figure 8
Macroscopic magnetization of a-$Fe_{1-x}Mn_x$ samples measured at T = 5 K up to magnetic fields of 5 T [data taken from Martin *et al.* (2021)].

which remain in the canted domains. SANS experiments in the medium and large Q range can explain how this process occurs microscopically. As shown in Fig. 9(a), the intensity measured in a 2D detector at T = 5 K and H = 1.5 T is strongly anisotropic, being enhanced in the direction $\mathbf{Q} \parallel \mathbf{H}$. Moreover, its radially averaged Q dependence shows a peak feature with a maximum at a finite value Q_{max} [Fig. 9(c)]. Both features show the existence of peculiar spin textures induced by the applied field and associated with small variations in the macroscopic magnetization.

The anisotropy and Q dependence of the neutron cross section can be used to deduce the characteristics of these textures, by virtue of the selection rule for magnetic neutron scattering. This stipulates that only magnetization components perpendicular to the scattering vector $\mathbf{Q}$ contribute to the observed cross section. Using this property, one can *e.g.* compute the cross section $\sigma_T(Q)$ corresponding to the moments transverse to the longitudinal magnetization by combining the scattered intensities recorded in sectors oriented $\parallel$ and $\perp$ to $\mathbf{Q}$. The Q dependence of $\sigma_T(Q)$ [Fig. 9(c)] suggests the presence of vortex-like defects, in which transverse spin components rotate over an average radius $\langle r_d \rangle = \pi/Q_{max}$ to compensate for the transverse magnetization within the texture. Monte Carlo simulations and toy models of the vortex structure factor confirm this interpretation (Mirebeau *et al.*, 2018; Martin *et al.*, 2021). They also show that the vortex-like defects have pancake shapes and nanometre sizes. Therefore, they clearly differ from the flux-line and skyrmion lattices observed in type II superconductors and itinerant ferromagnets perturbed by DM interactions, respectively. Both form long tubes across the samples, while the defects observed here are nucleated by and located around AFM Mn–Mn first-neighbour pairs.

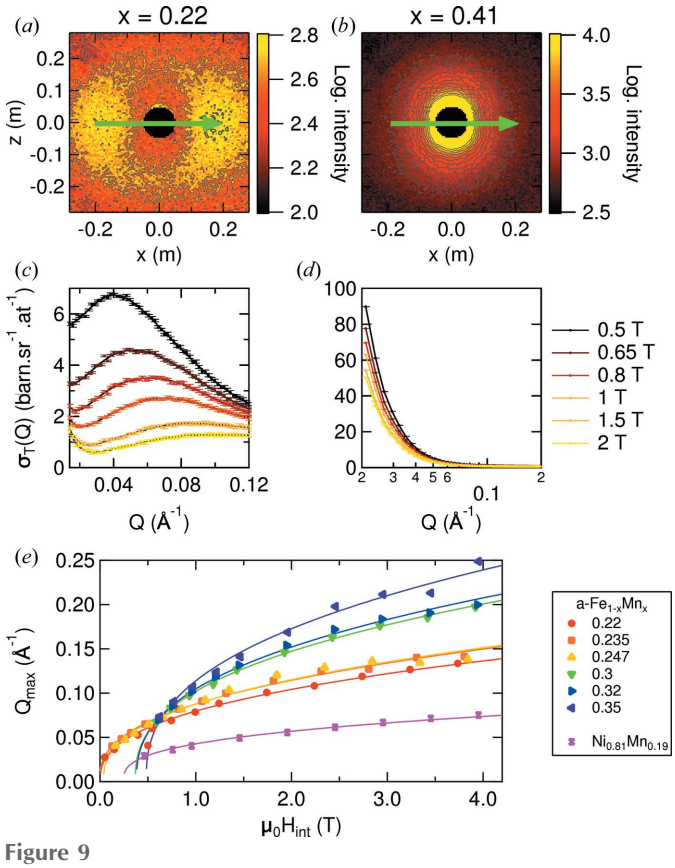

Figure 9
(a), (b) SANS data obtained at T = 5 K and H = 1.5 T in a-$Fe_{1-x}Mn_x$ with x = 0.22 and 0.41, respectively. Green arrows indicate the magnetic field direction. (c), (d) The 'transverse' magnetic cross section $\sigma_T(Q)$ deduced using the magnetic selection rule of neutron scattering from the data of panels (a) and (b), respectively (see text). (e) The scaling behaviour of the field-dependent position Q_{max} of the maximum in $\sigma_T(Q)$ for various a-$Fe_{1-x}Mn_x$ samples and $Ni_{0.81}Mn_{0.19}$. Data from all panels are taken from Martin *et al.* (2021).

As the Mn concentration increases, one goes from weakly frustrated RSGs (x = 0.22–0.26) to highly frustrated RSGs (x = 0.30–0.35) and finally to the SG sample (x = 0.41). The magnetization plateau is smeared in the highly frustrated RSGs, but the vortex persists in the whole RSG region up to $x_C \simeq 0.36$. In striking contrast, the intensity in the SG sample (x = 0.41) is enhanced in the direction $\mathbf{Q} \perp \mathbf{H}$ [Fig. 9(b)] and it decreases gradually with increasing Q, or H, without showing any maximum [Fig. 9(d)], while the magnetization plateau is no longer observed.

A detailed analysis of the SANS data measured for all samples (Martin *et al.*, 2021) helps in understanding the evolution of the magnetic ground state throughout the phase diagram. It can be summarized by considering the variation in Q_{max}, which determines the vortex size with H and x [Fig. 9(e)]. The vortices shrink when the magnetic field increases and 'swell' when the average ferromagnetic exchange constant J_0 increases, *i.e.* when x decreases [Fig. 2(b)]. The average vortex size obeys a scaling law of the type $Q_{max} \simeq H^{\beta}/J^{1/2}$, with $\beta \simeq 1/3$ (Martin *et al.*, 2021).

In the weakly frustrated samples, the vortices can be clearly distinguished from the domain walls by their smaller size and their persistence in high fields. They act as pinning centres, where the canting is locally enhanced, inducing a blocking of the domain wall mobility and a decrease in the low-field susceptibility. In the highly frustrated samples, discriminating between the magnetic scattering arising from different types of defect becomes less obvious, but small vortices clearly persist up to the critical concentration x_C.

The vortices vanish in the SG sample (x = 0.41), for which $\sigma_T(Q)$ displays a Q dependence similar to that of a paramagnet with FM correlations [Figs. 9(c) and 9(d)].

The combination of SANS with MC simulations shows two complementary phenomena: (i) the vortices emerge from an average ferromagnetic medium, acting as a vacuum field, and (ii) they protect the magnetic domains from breaking down under the influence of frustration. We note that similar SANS measurements, although less detailed, were performed in several other systems, namely $Au_{1-x}Fe_x$ (Lequien *et al.*, 1987), $Ni_{1-x}Mn_x$ (Mirebeau *et al.*, 2018) and $Fe_{1-x}Al_x$ (Böni *et al.*, 1986). All of them showed the presence of transverse magnetic defects, with similar line shapes for $\sigma_T(Q)$. Altogether, these results suggest that such defects are a characteristic feature of the mixed phases in RSGs, observed whatever the nature of the quenched disorder, magnetic interactions, crystal structure and sample form.

Finally, SANS studies performed with varying temperature show that the vortex textures persist up to the canting temperature T_k, as expected from their transverse nature. However, their observation when the temperature increases requires energy-resolved measurements to separate their contribution from that of the SWs. Up to now such energy-resolved measurements have been performed only in a weakly frustrated sample (x = 0.245) using TAS (M. Hennion *et al.*, 1986). Extending them to the highly frustrated samples would be a good test of the vertical critical line predicted by the GT model, as discussed above.

7. Summary and outlook

Through this review focused on two metallic systems, we have seen that neutron scattering and depolarization deliver key insight into the RSG problem, including static and dynamic properties. Among these methods, SANS is very well suited since it can probe the magnetic mesostructure of these disordered systems. Several questions remain, however, concerning the interpretation of the data and their relation to infinite-range models.

Recent technical developments could also help in clarifying some open issues and motivate new investigations over extended space and time ranges. In that spirit, we shall mention two classes of experiment relying on the use of polarized neutrons.

The first class is based on the spin echo small-angle neutron scattering (SESANS) technique (Rekveldt, 1996). SESANS renders the space Fourier transform of the scattering function up to 1–10 µm and, as such, bridges the gap between conventional SANS and imaging/microscopy. In particular, it allows monitoring of the domain properties of the RSG samples from the pure ferromagnet up to the strongly frustrated SG regime. Proof-of-principle experiments have indeed shown that the method works on depolarizing samples (Grigoriev *et al.*, 2006; Li *et al.*, 2021). An interesting development would be to make this technique also compatible with high magnetic fields at the sample position, in order to study the field-induced vortex-like defects discussed in Section 6 over an extended parameter range. This would be especially useful in the small magnetic field regime dominated by domains and domain walls, or in weakly frustrated RSGs where they are expected to be rather large objects.

A second class of experiments concerns accurate measurement of the spin dynamics of RSGs using MIEZE spectroscopy (Gähler *et al.*, 1992), which is a derivative of NSE allowing the study of the dynamic properties of condensed matter in a SANS geometry up to correlation times reaching a few tens of nanoseconds. The strength of MIEZE with respect to NSE is that its performance is not affected by depolarizing conditions, including ferromagnetic samples and large magnetic fields (Kindervater, *et al.*, 2015). As discussed in Section 4.1, SWs propagating in RSGs display properties which are at odds with those encountered in usual ordered magnets. A supplemental open question concerns their evolution under large magnetic fields, which probably involves the interaction between these SWs (collective excitations) and the vortices (localized defects) in the long-wavelength limit. One could encounter a non-trivial kind of 'magnonics', recalling that the size and density of these textures can be controlled by the applied field (Section 6).

The exploration of this phenomenology can be naturally extended to other RSGs, beyond the ones discussed in this paper. The Fe_xCr_{1-x} system, where the main interaction is either FM or AFM depending on x (Burke & Rainford, 1983*a*,*b*; Burke *et al.*, 1983), is most appealing. It would be interesting to search for vortex-like defects in the low-temperature mixed phases of the FM RSGs, situated in the Fe-rich phase. At low x content, the onset of AF Cr moments in the Fe matrix is well explained by the change in the band structure. It induces local canting, as a precursor effect of the RSG phase which occurs at higher x values (Mirebeau *et al.*, 2019). Alternatively, one could also search for another type of defect in the Cr-rich phase where AFM RSGs are observed. Such experiments will require the respective use of SANS and wide-angle diffraction, together with careful control of the sample's metallurgical state and macroscopic properties, considering that the chemical phase diagram is quite complex. However, by analogy with the search for AFM skyrmions (Gao *et al.*, 2020; Legrand *et al.*, 2020), this might be worth the effort.

There are certainly other lines of work which can be followed thanks to the continuous effort put into the improvement of neutron scattering and imaging methods. We believe that RSGs will fully benefit from these developments. Indeed, they still represent a vastly unexplored field of research, currently revitalized by the intense activities surrounding magnetic textures and topological defects in pure and applied condensed matter physics (Zang *et al.*, 2018).

References

Aeppli, G., Shapiro, S. M., Birgeneau, R. J. & Chen, H. S. (1982). *Phys. Rev. B*, **25**, 4882–4885.

Aeppli, G., Shapiro, S. M., Birgeneau, R. J. & Chen, H. S. (1984). *Phys. Rev. B*, **29**, 2589–2605.

Almeida, J. R. L. & Thouless, D. J. (1978). *J. Phys. A Math. Gen.* **11**, 983–990.

Anderson, P. (1988). *Phys. Today*, **41**, 9.

Beauvillain, P., Renard, J. P., Matecki, M. & Prejean, J. J. (1986). *Europhys. Lett.* **2**, 23–30.

Bellouard, C., Hennion, M., Mirebeau, I. & Hennion, B. (1992). *J. Magn. Magn. Mater.* **104–107**, 1627–1628.

Belokon', V. I., Nefedev, K. V. & Savunov, M. A. (2006). *Phys. Solid State*, **48**, 1746–1753.

Böni, P., Shapiro, S. & Motoya, K. (1986). *Solid State Commun.* **60**, 881–884.

Bouchiat, H. (1986). *J. Phys. Fr.* **47**, 71–88.

Brout, R. (1959). *Phys. Rev.* **115**, 824–835.

Burke, S. K., Cywinski, R., Davis, J. R. & Rainford, B. D. (1983). *J. Phys. F Met. Phys.* **13**, 451–470.

Burke, S. K. & Rainford, B. D. (1983*a*). *J. Phys. F Met. Phys.* **13**, 441–450.

Burke, S. K. & Rainford, B. D. (1983*b*). *J. Phys. F Met. Phys.* **13**, 471–482.

Cable, J. W. & Child, H. R. (1974). *Phys. Rev. B*, **10**, 4607–4615.

Cable, J. W., Werner, S. A., Felcher, G. P. & Wakabayashi, N. (1982). *Phys. Rev. Lett.* **49**, 829–832.
Cannella, V. & Mydosh, J. A. (1972). *Phys. Rev. B*, **6**, 4220–4237.
Castellani, T. & Cavagna, A. (2005). *J. Stat. Mech. Theory Exp.* **2005**, P05012.
Edwards, S. F. & Anderson, P. W. (1975). *J. Phys. F Met. Phys.* **5**, 965–974.
Fisher, D. S. & Huse, D. A. (1986). *Phys. Rev. Lett.* **56**, 1601–1604.
Gabay, M. & Toulouse, G. (1981). *Phys. Rev. Lett.* **47**, 201–204.
Gähler, R., Golub, R. & Keller, T. (1992). *Physica B*, **180–181**, 899–902.
Gao, S., Rosales, H. D., Gómez Albarracín, F. A., Tsurkan, V., Kaur, G., Fennell, T., Steffens, P., Boehm, M., Čermák, P., Schneidewind, A., Ressouche, E., Cabra, D. C., Rüegg, C. & Zaharko, O. (2020). *Nature*, **586**, 37–41.
Grigoriev, S. V., Kraan, W. H., Rekveldt, M. Th., Kruglov, T. & Bouwman, W. G. (2006). *J. Appl. Cryst.* **39**, 252–258.
Hadjoudj, S., Senoussi, S. & Mirebeau, I. (1991). *J. Magn. Magn. Mater.* **93**, 136–142.
Haetinger, C. M., Ghivelder, L., Schaf, J. & Pureur, P. (2009). *J. Phys. Condens. Matter*, **21**, 506006.
Halpern, O. & Holstein, T. (1941). *Phys. Rev.* **59**, 960–981.
Harders, T. M., Hicks, T. J. & Smith, J. H. (1983). *J. Phys. F Met. Phys.* **13**, 1263–1279.
Hartmann-Boutron, F. (1982). *J. Phys. Lett.* **43**, 853–859.
Hennion, B., Hennion, M., Hippert, F. & Murani, A. (1984). *J. Phys. F Met. Phys.* **14**, 489–504.
Hennion, B., Hennion, M., Mirebeau, I. & Hippert, F. (1986). *Physica B+C*, **136**, 49–52.
Hennion, M., Hennion, B., Mirebeau, I., Lequien, S. & Hippert, F. (1988). *J. Phys. Colloq.* **49**(C8), 1121–1126.
Hennion, M. & Mirebeau, I. (1995). *J. Magn. Magn. Mater.* **140–144**, 1565–1566.
Hennion, M., Mirebeau, I., Hennion, B., Lequien, S. & Hippert, F. (1986). *Europhys. Lett.* **2**, 393–399.
Hicks, T. J. (1983). *Aust. J. Phys.* **36**, 519–536.
Honecker, D., Bersweiler, M., Erokhin, S., Berkov, D., Chesnel, K., Venero, D. A., Qdemat, A., Disch, S., Jochum, J. K., Michels, A. & Bender, P. (2022). *Nanoscale Adv.* **4**, 1026–1059.
Kawamura, H. (1992). *Phys. Rev. Lett.* **68**, 3785–3788.
Kindervater, J., Martin, N., Häußler, W., Krautloher, M., Fuchs, C., Mühlbauer, S., Lim, J. A., Blackburn, E., Böni, P. & Pfleiderer, C. (2015). *EPJ Web Conf.* **83**, 03008.
Kustov, S., Torrens-Serra, J., Salje, E. K. H. & Beshers, D. N. (2017). *Sci. Rep.* **7**, 16846.
Lauer, J. & Keune, W. (1982). *Phys. Rev. Lett.* **48**, 1850–1853.
Lefloch, F., Hammann, J., Ocio, M. & Vincent, E. (1992). *Europhys. Lett.* **18**, 647–652.
Legrand, W., Maccariello, D., Ajejas, F., Collin, S., Vecchiola, A., Bouzehouane, K., Reyren, N., Cros, V. & Fert, A. (2020). *Nat. Mater.* **19**, 34–42.
Lequien, S., Hennion, B. & Shapiro, S. M. (1988). *Phys. Rev. B*, **38**, 2669–2674.
Lequien, S., Mirebeau, I., Hennion, M., Hennion, B., Hippert, F. & Murani, A. P. (1987). *Phys. Rev. B*, **35**, 7279–7282.
Li, F., Steinke, N. J., Dalgliesh, R. M., Washington, A. L., Shen, J., Pynn, R. & Parnell, S. R. (2021). *Nucl. Instrum. Methods Phys. Res. A*, **1014**, 165705.
Martin, N., Bannenberg, L. J., Deutsch, M., Pappas, C., Chaboussant, G., Cubitt, R. & Mirebeau, I. (2021). *Sci. Rep.* **11**, 20753.
Mezei, F. & Murani, A. (1979). *J. Magn. Magn. Mater.* **14**, 211–214.
Michels, A. (2021). *Magnetic Small-Angle Neutron Scattering: A Probe for Mesoscale Magnetism Analysis*. Oxford University Press.
Mirebeau, I. (1987). PhD thesis, Université de Paris-Sud, France.
Mirebeau, I., Hennion, M., Gingras, M. J. P., Keren, A., Kojima, K., Larkin, M., Luke, G. M., Nachumi, B., Wu, W. D., Uemura, Y. J., Campbell, I. A. & Morris, G. D. (1997). *Hyperfine Interact.* **104**, 343–348.
Mirebeau, I., Hennion, M., Mitsuda, S. & Endoh, Y. (1992). *Recent Progress in Random Magnets*, pp. 41–69 Singapore: World Scientific.
Mirebeau, I., Itoh, S., Mitsuda, S., Watanabe, T., Endoh, Y., Hennion, M. & Papoular, R. (1990). *Phys. Rev. B*, **41**, 11405–11416.
Mirebeau, I., Jehanno, G., Campbell, I., Hippert, F., Hennion, B. & Hennion, M. (1986). *J. Magn. Magn. Mater.* **54–57**, 99–100.
Mirebeau, I., Lequien, S., Hennion, M., Hippert, F. & Murani, A. (1989). *Physica B*, **156–157**, 201–204.
Mirebeau, I., Martin, N., Deutsch, M., Bannenberg, L. J., Pappas, C., Chaboussant, G., Cubitt, R., Decorse, C. & Leonov, A. O. (2018). *Phys. Rev. B*, **98**, 014420.
Mirebeau, I., Pierron-Bohnes, V., Decorse, C., Rivière, E., Fu, C.-C., Li, K., Parette, G. & Martin, N. (2019). *Phys. Rev. B*, **100**, 224406.
Mitsuda, S. & Endoh, Y. (1985). *J. Phys. Soc. Jpn*, **54**, 1570–1580.
Mitsuda, S., Yoshizawa, H., Watanabe, T., Itoh, S., Endoh, Y. & Mirebeau, I. (1991). *J. Phys. Soc. Jpn*, **60**, 1721–1729.
Mühlbauer, S., Honecker, D., Périgo, A., Bergner, F., Disch, S., Heinemann, A., Erokhin, S., Berkov, D., Leighton, C., Eskildsen, M. R. & Michels, A. (2019). *Rev. Mod. Phys.* **91**, 015004.
Murani, A. (1980). *Solid State Commun.* **34**, 705–708.
Mydosh, J. A. (2015). *Rep. Prog. Phys.* **78**, 052501.
Pappas, C., Alba, M., Brulet, A., Viel, V. & Mezei, F. (1996). *J. Appl. Phys.* **79**, 6158–6160.
Parisi, G. (1979). *Phys. Rev. Lett.* **43**, 1754–1756.
Rekveldt, M. (1996). *Nucl. Instrum. Methods Phys. Res. B*, **114**, 366–370.
Sato, T., Ando, T., Watanabe, T., Itoh, S., Endoh, Y. & Furusaka, M. (1993). *Phys. Rev. B*, **48**, 6074–6086.
Senoussi, S., Hadjoudj, S. & Fourmeaux, R. (1988). *Phys. Rev. Lett.* **61**, 1013–1016.
Sherrington, D. & Kirkpatrick, S. (1975). *Phys. Rev. Lett.* **35**, 1792–1796.
Souletie, J. (1978). *J. Phys. Colloq.* **39**, C2-3–C2-16.
Souletie, J. & Tholence, J. L. (1985). *Phys. Rev. B*, **32**, 516–519.
Souletie, J. & Tournier, R. (1969). *J. Low Temp. Phys.* **1**, 95–108.
Toninelli, F. L. (2002). *Europhys. Lett.* **60**, 764–767.
Toulouse, G. (1977). *Spin Glass Theory and Beyond*, pp. 99–103. Singapore: World Scientific.
Tsunoda, Y. & Cable, J. W. (1992). *Phys. Rev. B*, **46**, 930–936.
Uemura, Y. J., Harshman, D. R., Senba, M., Ansaldo, E. J. & Murani, A. P. (1984). *Phys. Rev. B*, **30**, 1606–1608.
Uemura, Y. J., Yamazaki, T., Hayano, R. S., Nakai, R. & Huang, C. Y. (1980). *Phys. Rev. Lett.* **45**, 583–587.
Vincent, E. & Dupuis, V. (2018). *Spin Glasses: Experimental Signatures and Salient Outcomes*, pp. 31–56. Cham: Springer International Publishing.
Wilhelm, F., Poulopoulos, P., Kapaklis, V., Kappler, J.-P., Jaouen, N., Rogalev, A., Yaresko, A. N. & Politis, C. (2008). *Phys. Rev. B*, **77**, 224414.
Yeshurun, Y., Salamon, M. B., Rao, K. V. & Chen, H. S. (1980). *Phys. Rev. Lett.* **45**, 1366–1369.
Zang, J., Cros, V. & Hoffmann, A. (2018). Editors. *Topology in Magnetism*. Heidelberg: Springer.